Article

Dynamic Mechanism for the Autophosphorylation of CheA Histidine Kinase: Molecular Dynamics Simulations

Jian Zhang, Yechun Xu, Jianhua Shen, Xiaomin Luo, Jiagao Chen, Kaixian Chen, Weiliang Zhu, and Hualiang Jiang

J. Am. Chem. Soc., **2005**, 127 (33), 11709-11719• DOI: 10.1021/ja051199o • Publication Date (Web): 27 July 2005

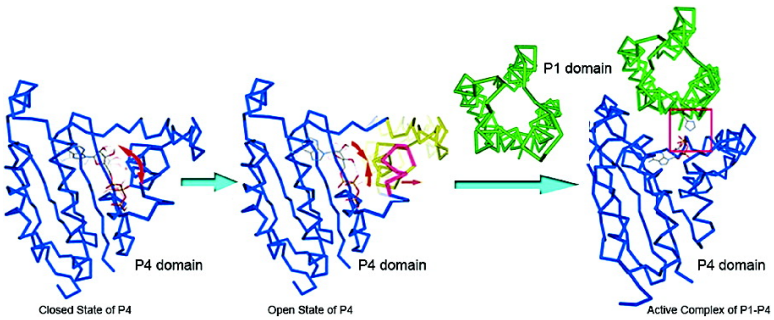

More About This Article

Additional resources and features associated with this article are available within the HTML version:

- Supporting Information
- Access to high resolution figures
- Links to articles and content related to this article
- Copyright permission to reproduce figures and/or text from this article

View the Full Text HTML

J|A|C|S
ARTICLES
Published on Web 07/27/2005

Dynamic Mechanism for the Autophosphorylation of CheA Histidine Kinase: Molecular Dynamics Simulations

Jian Zhang,[†] Yechun Xu,[†] Jianhua Shen,[†] Xiaomin Luo,[†] Jiagao Chen,[†] Kaixian Chen,[†] Weiliang Zhu,*[,†] and Hualiang Jiang*[,†,‡]

Contribution from the Center for Drug Discovery and Design, State Key Laboratory of Drug Research, Shanghai Institute of Materia Medica, Shanghai Institutes for Biological Sciences, and Graduate School, Chinese Academy of Sciences, 555 Zuchongzhi Road, Shanghai 201203, China, and School of Pharmacy, East China University of Science and Technology, Shanghai 200237, China

Received February 24, 2005; E-mail: wlzhu@mail.shcnc.ac.cn; hljiang@mail.shcnc.ac.cn

Abstract: The two-component system (TCS) is an important signal transduction component for most bacteria. This signaling pathway is mediated by histidine kinases via autophosphorylation between P1 and P4 domains. Taking chemotaxis protein CheA as a model of TCS, the autophosphorylation mechanism of the TCS histidine kinases has been investigated in this study by using a computational approach integrated homology modeling, ligand−protein docking, protein−protein docking, and molecular dynamics (MD) simulations. Four nanosecond-scale MD simulations were performed on the free P4 domain, P4−ATP, P4−TNPATP, and P1−P4−ATP complexes, respectively. Upon its binding to the binding pocket of P4 with a folded conformation, ATP gradually extends to an open state with help from a water molecule. Meanwhile, ATP forms two hydrogen bonds with His413 and Lys494 at this state. Because of the lower energy of the folded conformations, ATP shrinks back to its folded conformations, leading to the rupture of the hydrogen bond between ATP and Lys494. Consequently, Lys494 moves away from the pocket entrance, resulting in an open of the ATP lid of P4. It is the open state of P4 that can bind tightly to P1, where the His45 of P1 occupies a favorable position for its autophosphorylation from ATP. This indicates that ATP is not only a phosphoryl group donor but also an activator for CheA phosphorylation. Accordingly, a mechanism of the autophosphorylation of CheA is proposed as that the ATP conformational switch triggers the opening of the ATP lid of P4, leading to P1 binding tightly, and subsequently autophosphorylation from ATP to P1.

Introduction

The appearance of multiresistant and vancomycin-resistant *Staphylococcus epidermidis* (*S. epidermidis*) strains is a major problem in antibiotics discovery and development. Accordingly, identifying new targets for screening novel antibacterial agents is of importance.[1] The two-component system (TCS) signal transduction is a predominant signaling system mediated by histidine kinase in bacteria.[2,3] TCSs are crucial to bacteria, for they modulate a large variety of bacterial characteristics, such as chemotaxis, virulence, osmoregulation, autolysis, competence formation, and growth regulation.[3−5] In addition, TCSs are rarely found in mammalians. Therefore, enzymes involved in TCSs may be attractive targets for discovering new compounds that may selectively inhibit the growth of prokaryote.[6,7] TCSs are proteins composed of two or more multidomains, which can be categorized in two classes based on their distinct pathways of histidine autophosphorylation and transphosphorylation.[8,9] The TCSs associated with bacterial chemotaxis belongs to the second class (class II) of TCSs, which have been well studied to date (Figure 1).[10,11]

Several proteins are involved in the signal transduction in the TCS of chemotaxis system as demonstrated in Figure 1. In this signaling pathway, a protein called CheA plays a role of histidine autokinase and serves as a core.[12] First, CheA is modulated by a membrane-bound sensor receptor (SENSOR) via a coupling protein (CheW). Then, CheA transfers a phosphoryl group to a regulator protein (CheY), which functions as a transducer through interacting with effectors for downstream signal transduction.[13] Structurally, CheA contains 5 domains, i.e., the P1−P5 domains (P1−P5 hereinafter for clarity, Figure 1). P1 possesses of a conserved histidine residue. Autophosporylation occurs from ATP in the active site of P4 to His45 of

[†] Chinese Academy of Sciences.
[‡] East China University of Science and Technology.

(1) Duncan, K. *Curr. Pharm Des.* **2004**, *10* (26), 3185−3194.
(2) Stock, J. B.; Ninfa, A. J.; Stock, A. M. *Microbiol. Rev.* **1989**, *53*, 450−490.
(3) Parkinson, J. S.; Kofoid, E. C. *Annu. Rev. Genet.* **1992**, *26*, 71−112.
(4) Galperin, M. Y.; Nikolskaya, A. N.; Koonin, E. V. *FEMS Microbiol. Lett.* **2001**, *203*, 11−21.
(5) Appleby, J. L.; Parkinson, J. S.; Bourret, R. B. *Cell* **1996**, *86*, 845−848.
(6) Ban, C.; Junop, M.; Yang, W. *Cell* **1999**, *97*, 85−97.
(7) Hess, J. F.; Oosawa, K.; Kaplan, N.; Simon, M. I. *Cell* **1988**, *53*, 79−87.
(8) Koretke, K. K.; Lupas, A. N.; Warren, P. V.; Rosenberg, M.; Brown, J. R. *Mol. Biol. Evol.* **2000**, *17*, 1956−1970.
(9) Matsushita, M.; Janda, K. D. *Bioorg. Med. Chem.* **2002**, *10*, 855−867.
(10) Bilwes, A. M.; Alex, L. A.; Crane, B. R.; Simon, M. I. *Cell* **1999**, *96*, 131−141.
(11) Bilwes, A. M.; Quezada, C. M.; Croal, L. R.; Crane, B. R.; Simon, M. I. *Nat. Struct. Biol.* **2001**, *8*, 353−360.
(12) Dutta, R.; Qin, L.; Inouye, M. *Mol. Microbiol.* **1999**, *34*, 633−640.
(13) Djordjevic, S.; Stock, A. M. *J. Struct. Biol.* **1998**, *124*, 189−200.

10.1021/ja051199o CCC: $30.25

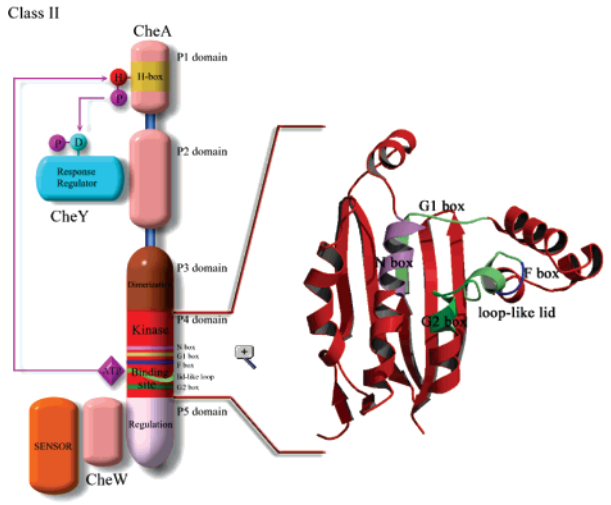

Figure 1. Composition of class II TCSs (left) and structural feature of the P4 domain in CheA (right). P represents phosphate, D stands for aspartic acid in the response regulator, and H is the histidine in the H box. Arrow represents the flow of phosphate through this system.

P1, followed by transphosphorylation from the histidine residue to an aspartate residue of CheY. P2 is a specific domain for recognizing CheY and assists transfer of the phosphoryl group. P5 acts as a regulative domain to modulate the activity of autotransphophorylation, responding signals from external environment via the coupling protein CheW. P3 is a linking domain, through which two CheA subunits form a dimer. P4 is an ATP binding domain, which autophosphorylates the conserved histidine residue (His45) of P1. In general, P4 is composed of five stranded β-sheets and four α-helices,[10,14] forming a two-layered α/β sandwich structure (Figure 1). Most of the residues around the ATP binding site of P4 are conserved, especially those consisting of N (plum), G1 (pale green), F (blue), and G2 (green) boxes (Figure 1, right).[11] In addition, P4 has a looplike lid (ATP lid) between the F and G2 boxes (light green) that controls the closed-to-open change of the binding pocket.

The autophosphorylation of His45 of P1 by the ATP from P4 initiates the signal transduction in TCS. Thus, understanding the mechanism of the autophosphorylation is of significance, especially in designing new antibiotics to treat multiresistant bacteria. Although recent works have provided some insights into the autophosphorylation reaction,[15−20] several fundamental questions are still open. In particular, what causes the conformational change of ATP within the binding site? How does the ATP lid open so that the autophosphorylation occurs from the ATP in the binding site of P4 to His45 of P1? Why can TNPATP (2′(3′)-O-(2,4,6-trinitrophenyl)−adenosine 5′-triphosphate), a very similar nucleotide analogue of ATP, bind to the active site tightly but its phosphoryl group cannot be transferred to His45 of P1?[21] To reach the answers of these questions, we have performed a series of molecular modeling and molecular dynamics (MD) simulations on free P4, P4−ATP complex, and P4−TNPATP complex. In the following, we report on the modeling and MD results for the dynamic mechanism of the autophosphorylation from ATP to His45 in the CheA histidine kinase.

Computational Procedure

As mentioned above, CheA consists of 5 domains (P1−P5), and autophosphorylation occurs between P1 and P4 domains. This study focuses on the conformational change of P4 stimulated by ATP and the correlation between P1−P4 interaction and CheA autophosphorylation. However, only the X-ray crystal structures of the P4 of *T. maritime* and P1 of *S. typhimurium* have been determined.[10,11,22] The experimental structures of P1 and P4 from one bacterial species are not available to date, much less the structure of P1−P4 complex.[23,24] To solve these problems, we integrated several modeling and simulation methods in this study. The computational pipeline is outlined in Figure S1 in the Supporting Information. Briefly, the computational flow is as follows. (1) The ligand−protein docking approach was used to construct a 3D model of P4−ATP complex based on the X-ray crystal structure of P4−ADPCP complex (1I58);[11] meanwhile, a 3D model of the *T. maritime* P1 was generated by means of homology modeling using the X-ray structure of the *S. typhimurium* P1 as a template. (2) A 4-ns MD simulation was carried out on the P4−ATP complex model, and two 4-ns MD simulations were performed in parallel on free P4 and the P4−TNPATP complex to address the dynamics difference of ATP-induced P4 to free P4 and P4 induced by inhibitors; complementarily, principal-component analyses (PCA) were carried out on the MD trajectories in order to identify the most significant fluctuation modes of the proteins. (3) A 3D model of the P1−P4 complex was built up by docking the P1 3D model to an open conformation of P4−ATP complex with the protein−protein docking method, and a 2-ns MD simulation was also conducted on the P1−P4 complex model.

Molecular Models of P4 and Its Ligand Complexes. The models of P4 and its substrate complexes for the MD simulations were constructed based on the X-ray crystal structures of free CheA P4 (1B3Q, resolution 2.6 Å),[10] P4−ADPCP complex (1I58, resolution 1.6 Å)[11] and P4−TNPATP complex (1I5D, resolution 2.9 Å).[11] The side chains with missing coordinates were reconstructed using the fragment library of the Biopolymer module in Sybyl version 6.8 (Tripos Inc.St. Louis, MO).[25] The modified structures were subjected to energy minimization in Sybyl6.8 using the steepest descent method up to the gradient tolerance of 0.05 kcal/(mol·Å) to relieve possible steric clashes and overlaps of side chains.

The 3D structural model of P4−ATP complex was built up based on the X-ray crystal structure of CheA P4−ADPCP complex (1I58).[11] Residues around the ADPCP within 5 Å, which is larger enough to include the binding site, were extracted to comprise the binding pocket for docking. The possibly best binding pose (orientation and conformation) of ATP binding to P4 was searched using the DOCK4.0 program.[26,27] During the docking simulation, Kollman all-atom charges[28] were assigned to the protein, and Gasterger−Hückel charges[29−31] were assigned to ATP.

Homology Modeling for the 3D Model of P1. The X-ray crystal structure of the P1 domain of *Salmonella typhimurium* (*S. typhimurium*)

(14) Ikura, M. et al. *Nature* **1998**, *396*, 88−92 (ref S1, Supporting Information).
(15) Swanson, R. V.; Schuster, S. C.; Simon, M. I. *Biochemistry* **1993**, *32*, 7623−7629.
(16) Levit, M.; Liu, Y.; Surette, M.; Stock, J. *J. Biol. Chem.* **1996**, *271*, 32057−32063.
(17) Wolfe, A. J.; McNamara, B. P.; Stewart, R. C. *J. Bacteriol.* **1994**, *176*, 4483−4491.
(18) Surette, M. G.; Levit, M.; Liu, Y.; Lukat, G.; Ninfa, E. G.; Ninfa, A.; Stock, J. B. *J. Biol. Chem.* **1996**, *271*, 939−945.
(19) Tawa, P.; Stewart, R. C. *Biochemistry* **1994**, *33*, 7917−7924.
(20) Tawa, P.; Stewart, R. C. *J. Bacteriol.* **1994**, *176*, 4210−4218.
(21) Stewart, R. C.; VanBruggen, R.; Ellefson, D. D.; Wolfe, A. J. *Biochemistry* **1998**, *37*, 12269−12279.
(22) Mourey, L.; Da Re. S. *J. Biol. Chem.* **2001**, 276(33), 31074−31082.
(23) Garzon, A.; Parkinson, J. S. *J. Bacteriol.* **1996**, *178*, 6752−6758.
(24) Levit, M. N.; Liu, Y.; Stock, J. B. *Biochemistry* **1999**, *38*, 6651−6658.
(25) *Tripos*, 6.8 ed.; Tripos Inc.: St. Louis, MO, 2001.
(26) Kuntz, I. D. *Science* **1992**, *257*, 1078−1082.
(27) Ewing, T. J.; Kuntz, I. D. *J. Comput. Chem.* **1997**, *18*, 1175−1189.
(28) Cornell, W. D.; Cieplak, D. P.; Bayly, C. I.; Gould, I. R.; Merz, K. M.; Ferguson, D. M. *J. Am. Chem. Soc.* **1995**, *117*, 5179−5197.
(29) Purcell, W. P.; Singer, J. A. *J. Chem. Eng. Data* **1967**, *12*, 235−246.
(30) Marsili, M.; Gasteriger, J. *Croat. Chem. Acta* **1980**, *53*, 601−614.
(31) Gasteiger, J.; Marsili, M. *Tetrahedron* **1980**, *36*, 3219−3228.

(1I5N, resolution 2.1 Å)[22] was used as a template to construct the 3D model of the P1 of *Thermotoga maritime* (*T. maritime*). The sequence of the P1 domain of *T. maritime* was retrieved from the GenBank (Q56310) (http://www.ncbi.nlm.nih.gov/). The Align 2D module encoded in Insight II (Accelrys Corporate, San Diego, CA)[32] was used for the pairwise alignment.[33] According to the secondary structure information of the template, the sequence alignment was adjusted manually to obtain a more reasonable alignment. Then, a 3D model of the P1 of *T. maritime* was generated by using the program MODELLER[34] encoded in Insight II. MODELLER yielded three models, each of which contains three optimizing loop structures. The structure with the lowest violation and energy scores was chosen as the candidate. Refine routine in the Homology module of InsightII was used to adjust the positions of the side chains. Finally, the constructed model was optimized using AMBER force field[28] with the following parameters: a distance-dependent dielectric constant of 4.0, nonbonded cutoff 8 Å, Kollman all-atom charges.[28] The structure was minimized by steepest descent first, followed by conjugate gradient method to the energy gradient root-mean-square (RMS) <0.05 kcal/(mol·Å). The final structure was checked and validated by several programs such as Prostat and Profile-3D.[35]

Construction for the 3D Model of P1−P4−ATP Complex. The protein−protein docking program, 3D-DOCK,[36−38] was applied to construct a 3D model of P1−P4−ATP complex for further MD simulation. The homology model of P1 constructed by above method and an appropriate conformation isolated from the MD trajectory of P4−ATP complex were used during the P1−P4 docking. Briefly, the overall algorithm of 3D-DOCK is achieved in 4 steps: (1) globally scan the translational and rotational spaces of the two proteins to identify possible interaction positions, limited by surface complementarity and an electrostatic filter; (2) score the possible complex pairs using the empirical function developed based on the residue level pair potentials; (3) evaluate the possible complex configurations using the available biological information; (4) perform energy minimization for the protein−protein complex candidates to remove the steric clash between side chains of the interface.

MD Simulations. The MD simulations were preformed using the GROMACS package version 3.1.4[39−41] with the GROMOS96 force field.[42,43] The molecular topology files for ATP and TNPATP were generated by the program PRODRG[44] (http://davapc1.bioch.dundee.ac.uk/programs/prodrg/prodrg.html). The partial atomic charges of ATP and TNPATP were determined by using the CHelpG method[45] implemented in the Gaussin98 program[46] at the level of HF/6-31G*. For MD simulations, the four models (free P4, P4−ATP, P4−TNPATP, and P1−P4−ATP complexes) were solvated with the simple point charge (SPC) water model.[47] To maintain the systems at a constant temperature of 300 K, the Berendsen thermostat[48] was applied using a coupling time of 0.1 ps. The pressure was maintained by coupling to a reference pressure of 1 bar. A coupling time of 1.0 ps was used for the simulations in bulk water.[48] The values of the isothermal compressibility were set to 4.5×10^{-5} bar^{-1} for water simulations. All bond lengths including hydrogen atoms were constrained by the LINCS algorithm.[49] Electrostatic interactions between charge groups at a distance less than 9 Å were calculated explicitly; long-range electrostatic interactions were calculated using the particle−mesh Ewald method[50] with a grid width of 1.2 Å and a fourth-order spline interpolation. A cutoff distance of 14 Å was applied for the Lennard-Jones interactions. For each system, the simulation cell was a rectangular periodic box, the minimum distance between the protein and the box walls was set to more than 8 Å so that the protein does not directly interact with its own periodic image given the cutoff in every system. Numerical integration of the equations of motion used a time step of 2 fs with atomic coordinates saved every 10 ps for analysis. To neutralize the modeled systems, 1, 4, 5, and 12 water molecules were replaced by 1 Cl^-, 4 Na^+, 5 Na^+, and 12 Na^+ ions in the systems of free P4, P4−ATP, P4−TNPATP, and P1−P4−ATP complexes, respectively. These ions were located at positions of the chosen water oxygen atoms. At the end, the simulation system for free P4 is totally composed of 1869 protein atoms and 9695 solvent molecules embedded in a $6.2 \times 6.8 \times 7.5$ nm^3 box, the P4−ATP system the contains 1893 solute atoms and 7610 solvent molecules embedded in a $6.9 \times 5.7 \times 6.6$ nm^3 box, P4−TNPATP system is consisted of 1926 solute atoms and 9354 solvent molecules embedded in a $6.4 \times 5.9 \times 8.2$ nm^3 box, and the P1−P4−ATP system includes 2911 solute atoms and 16198 solvent molecules embedded in a $8.9 \times 8.3 \times 7.2$ nm^3 box. All water molecules and ions in the simulation models were minimized with protein structures fixed by using the steepest descent method to the convergence criterion of 100 kJ/(mol·nm), followed by energy minimizations on the whole systems but with protein main-chain and C^α atoms fixed. Water molecules, proteins, and ligands were coupled separately to a temperature bath at 300 K using a coupling time of 0.1 ps. Finally, three 4-ns MD and one 2-ns simulation were performed on these systems, respectively.

PCA. PCA was carried out in order to identify the most significant fluctuation modes of the proteins. PCA is based on the calculation of diagonalization of the covariance matrix *C*, whose elements are defined as

$$C_i = \langle (x_i - \langle x_i \rangle)(x_j - \langle x_j \rangle) \rangle \quad (i, j = 1, 2, 3, ..., 3N) \qquad (1)$$

where x_i is a Cartesian coordinate of the *i*th C^α atom, *N* is the number of the C^α atoms considered, and $\langle x_i \rangle$ represents the time average over all the configurations obtained in the simulation. The eigenvectors of the covariance matrix, υ_k, obtained by solving $\upsilon_k^T C \upsilon_k = \lambda_k$, stand for a set of 3*N*-dimensional directions, or principal modes, along which the fluctuations observed in the simulation are uncoupled with respect to each other (i.e., $C_{ij} = 0$ if $i \neq j$), and thus can be analyzed separately. The central hypothesis of this method is that only the motions along the eigenvectors with large eigenvalues are important for describing the functionally significant motions in the protein.[51−53] Domain motion analyses based on the PCA results were performed using the DYNDOM program.[54,55]

(32) *Accelrys*, 2000 ed.; Accelrys Inc.: San Diego, 2000.
(33) Thompson, J. D.; Higgins, D. G.; Gibson, T. J. *Nucleic Acids Res.* **1994**, *22*, 4673−4680.
(34) Sali, A.; Blundell, T. L. *J. Mol. Biol.* **1993**, *234*, 779−815.
(35) Bowie, J. U.; Luthy, R.; Eisenberg, D. *Science* **1991**, *253*, 164−170.
(36) Moont, G.; Gabb, H. A.; Sternberg, M. J. *Proteins* **1999**, *35*, 364−373.
(37) Jackson, R. M.; Gabb, H. A.; Sternberg, M. J. *J. Mol. Biol.* **1998**, *276*, 265−285.
(38) Gabb, H. A.; Jackson, R. M.; Sternberg, M. J. *J. Mol. Biol.* **1997**, *272*, 106−120.
(39) Berendsen, H. J. C.; D. van der Spoel; Drunen, R. v. *Comput. Phys. Commun.* **1995**, *91*, 43−56.
(40) Lindahl., E.; Hess, B.; van der Spoel, D. *J. Mol. Mod.* **2001**, *7*, 306−317.
(41) Berendsen, H. J. C. et al. 3.1 ed.; Nijenborgh, AG Groningen, The Netherlands, www.gromacs.org, 2002 (ref S2, Supporting Informtion).
(42) van der Spoel, D.; Buuren, A. R. v.; Tieleman, D. P.; Berendsen, H. J. *J. Biomol. NMR* **1996**, *8*, 229−238.
(43) van Gunsteren, W. F.; Berendsen, H. J. **1987**.
(44) Van Aalten, D. M. F.; Bywater, R.; Findlay, J. B. C.; Hendlich, M.; Hooft, R. W. W.; Vriend., G. *J. Comput.-Aided Mol. Des.* **1996**, *10*, 255−262.
(45) Breneman, C. M.; Wiberg, K. B. Determining atom-centered monoploes from molecular electrostatic potentials. *J. Comput. Chem.* **1990**, 11, 361−397.
(46) Frisch, M. J. et al. *Gaussian 98*, revision A.7; Gaussian, Inc.: Pittsburgh, PA, 1998. (Reference S3, Supporting Information)
(47) Interaction models for water in relation to protein hydration. In *Intermolecular Forces*; Berendsen, H. J. C., Postma, J. P. M., Gunsteren, W. F. v., Hermans, J., Eds. D. Reidel Publishing Company: Dordrecht, The Netherlands, 1981.
(48) Berendsen, H. J. C.; Postma, J. P. M.; Gunsteren, W. F. v.; DiNola, A.; Haak, J. R. *J. Chem. Phys* **1984**, *81*, 3684−3690.
(49) Hess, B.; Bekker, H.; Berendsen, H. J. C.; Fraaije, J. G. E. M. *J. Comput. Chem.* **1997**, *18*, 1463−1472.
(50) Darden, T.; D. York; Pedersen, L. *J. Chem. Phys* **1993**, *98*, 10089−10092.
(51) Kitao, A.; Go, N. *Curr. Opin. Struct. Biol* **1999**, *9*, 164−169.
(52) Amadei, A.; Linssen, A. B. M.; Berendsen, H. J. C. *Struct. Funct. Genet* **1993**, *17*, 412−425.
(53) Hayward, S.; Go, N. *Annu. Rev. Phys. Chem* **1995**, *46*, 223−250.
(54) Hayward, S., A.; Kitao, H. J. C.; Berendsen, H. J. *Proteins* **1997**, *27*, 425−437.
(55) Hayward, S.; Berendsen, H. J. *Proteins* **1998**, *30*, 144−154.

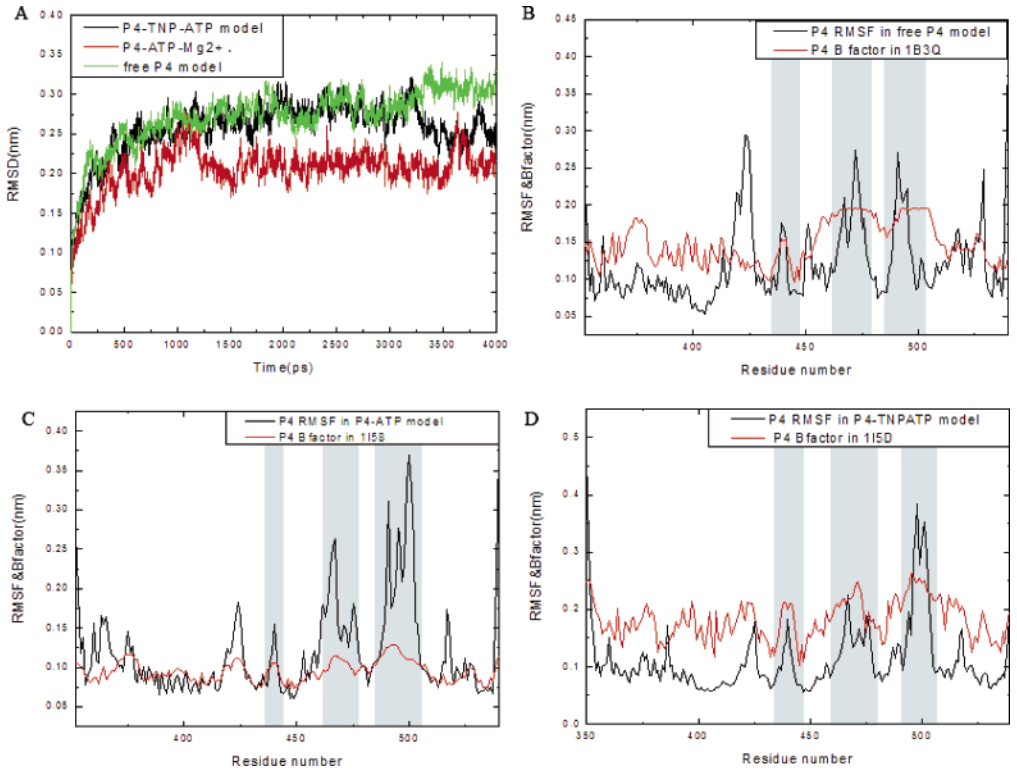

Figure 2. Time dependence of the RMSDs from the crystal structures of P4 and its substrate complexes for the C^{α} atoms in the 4-ns MD simulations (A). Residue fluctuations obtained by averaging atomic fluctuations over the 4-ns simulation (black curves) and by computing the value from the experimentally derived B factors (red curves) for P4 (B), the P4−ATP complex (C), and the P4−TNPATP complex (D). The highly flexible loops between the residues 440 and 506 are highlighted.

Results

Binding Model of ATP to P4. As ATP always tends to be hydrolyzed in situ, it is difficult to determine the 3D structure of P4−ATP complex. Thus Alexandrine et al. determined the X-ray structure of CheA P4−ADPCP complex, in which ADPCP was used to mimic ATP.[11] Therefore, we built up a structural model for P4-ATP complex using the DOCK4.0 program[26,27] based on the X-ray crystal structure of CheA P4−ADPCP complex (1I58).[11] The binding model of ATP to P4 is extremely similar to that of ADPCP in the crystal structure (Figure S2 in the Supporting Information). The adenosine ring was deeply embedded in the hydrophobic area of the binding site, and the phosphate tail points toward the entrance of the binding site. The RMS deviation (RMSD) between the binding conformations of ATP and ADPCP is below 0.55 Å. This result is in good agreement with experimental conclusion that ADPCP is a complete substitute for ATP in terms of binding pattern,[11] suggesting that our P4−ATP model derived from docking simulation is reliable; thereby it can be used for further MD simulations.

The Stability and Flexibility of the Overall Protein Structures. The MD simulation on the P4−ATP complex showed that the binding site of P4 was completely opened at ~3 ns (data not shown). Thus, 4-ns MD simulations are enough for discussing the dynamics of P4, P4−ATP, and P4−TNP−ATP. For all of the systems, the temperature, total energy, mass density, and volume are relatively stable during the 4-ns simulation period, suggesting that the simulations were carried out satisfyingly. Figure 2A shows the RMSDs from the crystal structures of C^{α} atoms vs simulation time. As shown in Figure 2A, after ~0.5 ns, the RMSD of each system tends to be convergent, indicating the system is stable and the system has been equilibrated.

The time evolution of the RMS fluctuation (RMSF) from the averaged structure provides another approach to evaluate the convergence of the dynamical properties of the system. Parts B−D of Figure 2 show the atomic fluctuations averaged over residues for the three P4-related systems derived from the 4-ns MD trajectories. For comparison, the corresponding values of RMSFs obtained from the experimental B factors in crystal structures are also shown in parts B−D of Figure 2. The experimental B factors are transformed to the RMSF with the formula $\langle \Delta r_i^2 \rangle = 3B_i/(8\pi^2)$.[56] RMSF profiles indicate that the residues with higher fluctuation values are those in the long loop Asp449−Gly506; this is in agreement with the experimental results reflected by the B factors derived from the X-ray crystallographic data,[11] indicating the reasonability of our MD results.

Conformations of ATP in the Binding Site. Figure 3A shows that the RMSDs of ATP and TNPATP inside the binding pocket of P4 vs simulation time. Interestingly, the RMSD of ATP remains below ~0.6 Å during the first 1.5 ns, it reaches ~1.5 Å in the following 1.5 ns, afterward, and it descends back to ~0.6 Å again. This result reveals that ATP may switch between two kinds of conformations in the binding site of P4 (Figure 3B). Different from that of ATP, the RMSD of TNPATP within the binding pocket of P4 has no obvious fluctuations during the simulation time, indicating that the conformation of TNPATP does not change dramatically during the MD simulation (Figure 3C). The difference in chemical structures between

(56) Wlodek, S. T.; Clark, T. W.; Scott, R.; McCammon. *J. Am. Chem. Soc.* **1997**, *119*, 9513−9522

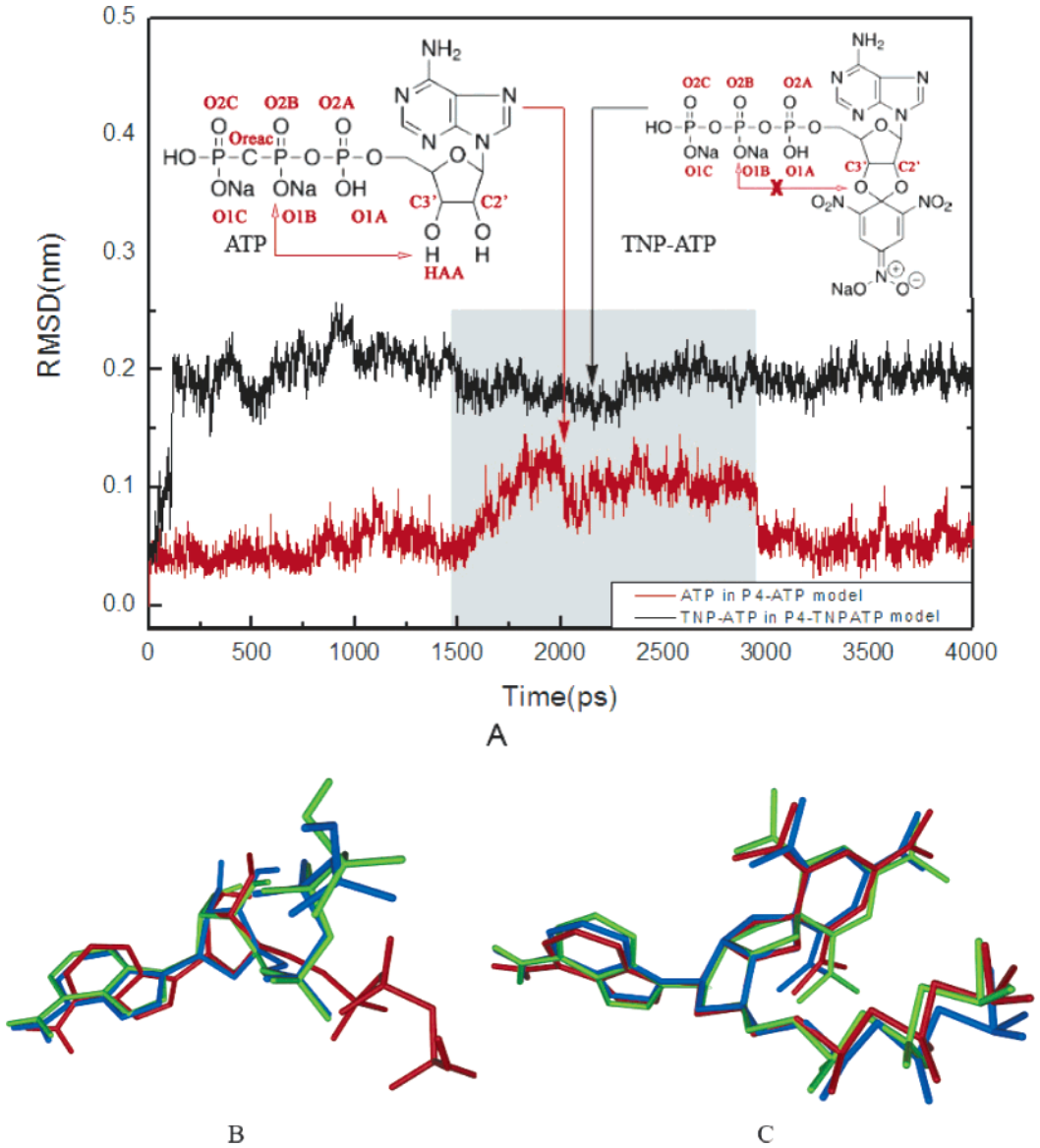

Figure 3. (A) RMSDs of ATP and TNPATP inside the binding site of P4 vs simulation time. (B) Structural superposition for the typical snapshots of ATP isolated from the MD trajectory: 500 ps (blue), 2000 ps (red), 3000 ps (green). (C) Structural superposition for the typical snapshots of TNPATP isolated from the MD trajectory: 1000 ps (blue), 2000 ps (red), 3000 ps (green).

ATP and TNPATP is in the sugar ring (Figure 3A).[21] The C2′ and C3′ atoms in the sugar ring of ATP, respectively, possess two free hydroxyls, 2′OH and 3′OH. While in TNPATP, these two hydroxyls cyclized with a trinitrobezene. Therefore, the spiral ring leads to the conformational rigidity of TNPATP in the binding site of P4 (see discussion below).

Hydrogen Bond Controls the Conformational Switch of ATP. Structurally, the hydrogen atom of 3′OH (HAA) may form an intramolecular hydrogen bond (H bond) with the oxygen atom attached to β-phosphate (O1B or O2B) of ATP (Figure 3A). This H bond might play an important role for the conformational switch of ATP. Accordingly, we monitored the distance of HAA to O1B and O2B along the simulation time, the results are shown in Figure 4. Obviously, HAA of ATP forms a H bond to O1B in the period of 0−1.6 ns, except abolished for a while (from 1.0 to 1.25 ns). However, the H bond was broken from 1.6 to 3.0 ns. Afterward, the H bond was recovered again. This H-bond profile exactly matches the RMSD of ATP, which reflects the ATP conformational change inside the binding pocket (Figure 3A). The H bond between HAA and O1B allows ATP to adopt folded conformations with lower RMSDs relative to the X-ray crystal structure (the first 1.6 ns and the period from 3.0 to 4.0 ns); while the H-bond breaking (1.6−3.0 ns) allows ATP to adopt extended conformations, leading to large RMSDs (Figures 3 and 4). Therefore, it seems that the H-bond making and breaking between HAA and O1B control the conformational switch of ATP in the binding pocket, further stimulating the conformational change of P4, especially the ATP lid (see discussion below).

A Water Molecule Mediates ATP Conformational Switch. The X-ray crystal structure of P4−ADPCP complex indicated that an array of water molecules play an important role for the stustrate−P4 binding.[11] To study the roles of water molecules in the binding of ATP to P4 and in the conformational switch of ATP, we performed a detailed analysis for the MD trajectory of P4−ATP systems by using the VMD program.[57] Figure 5 shows one snapshot isolated from the MD trajectory. MD simulation result indicates that, similar to the binding between

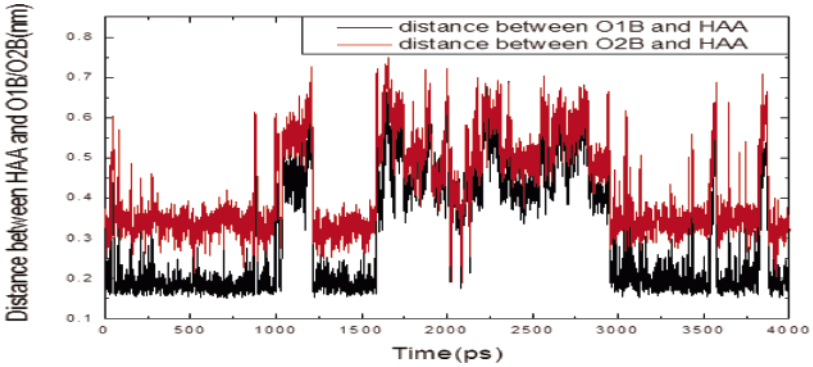

Figure 4. Time dependences the distances of HAA to O1B and O2B.

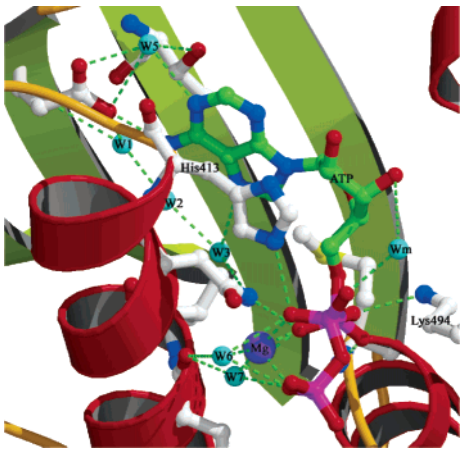

Figure 5. Interaction between P4 and ATP with 6 water molecules, W1, W2, W3, W5, W6, and W7, as named by Alexandrine et al.[11] The distance between residues His413 and Lys494 reflect the width of binding site. Green dashed lines represent hydrogen bonds or salt bridges between two atoms.

P4 and ADPCP, six water molecules (W1−W3 and W5−W7 in Figure 5) form a network through H bonds, which bridge the interactions of ATP to P4 and the magnesium ion, enhancing the binding between ATP and P4.

Noticeably, in addition to above six water molecules around ATP, HAA and O1B of ATP is bridged by a water molecule (Wm, Figure 5) from the solvent when ATP behaves as extended conformations within the P4 binding pocket (from 1.6 to 3.0 ns). During this period, ATP forms a H bond with Lys494 of P4. This water molecule gradually inserts between HAA and O1B from 1.6 to 2.0 ns, then the inserted water molecule leaves away from ATP, and ATP stretches to an extended conformation. ATP vibrates with extended conformations inside the P4 binding pocket till ∼3.0 ns. At this time, ATP suddenly shrinks back and HAA hydrogen bonds directly to O1B once again, which ruptures the H bond between ATP and Lys494. This indicates that Wm may play a significant role for the conformational switch of ATP in the P4 binding pocket. To confirm this postulation, the probable transition states for the ATP conformational switch without and with a water molecule inserting between HAA and O1B were identified using the density-functional quantum chemical method B3LYP/6-31G*.[46] The computational detail is described in the Supporting Information (Appendix I), and the result is shown in Figure S3 in the Supporting Information. The activation energy was estimated as ∼17.38 kcal/mol for the ATP conformational switch from a folded conformation to an extended conformation without the help of a water molecule. However, with the mediation of a water molecule the activation energy decreased to ∼13.05 kcal/mol, indicating that the water molecule (Wm in Figure 5) bridging HAA and O1B lowers the energy barrier for the ATP conformational change by ∼4.33 kcal/mol. This clearly demonstrates the function of Wm for the conformational switch of ATP. In additional, the quantum chemical calculation reveals that the folded conformation of ATP is ∼6.40 kcal/mol (ca. the strength of a typical H bond) more stable than the extended conformation, suggesting that the conformational outspread of ATP from the folded conformations to extended conformations is thermodynamically unfavorable and that the conformational shrinking of ATP from extended conformations to folded conformations (at ∼3.0 ns) is a thermodynamically favorable process. This result indicates that the process from folded conformations to extended conformations is slower than the reverse process. Indeed, MD simulation result is in agreement with the quantum chemical calculation, the outspreading process of ATP takes ∼0.5 ns (1.5−2.0 ns), but the shrinking process is quickly accessed (at ∼3.0) (Figure 3A).

Closed-to-Open Change of the ATP Lid. ATP lid plays an important role for the autophosphorylation of the histidine kinase of the class II.[58,59] Mutations for several residues of ATP lid completely eliminated the autophosphorylation activity of the histidine kinase; however, these mutations did not affect ATP binding affinity.[55] Nevertheless, the X-ray structures of P4 and its substrate mimic complexes did not give the reason why the ATP lid is associated with the autophosphorylation function of ChA. To this end, we investigated the dynamic property of the ATP lid based on the MD simulations.

Mutagenesis studies indicate that His413 and Lys494 are important residues for the CheA autophosphorylation function.[7,59] Crystal structures demonstrate that these two residues are located at two sides of ATP binding pocket entrance, controlling the width of the entrance.[11] In addition, Lys494 is a key residue at ATP lid.[11] To obtain an dynamic feature of the binding pocket entrance, the minimum van der Waals distances between His413 and Lys494 (H−K distance) were monitored during the MD simulations. Figure 6 displays the fluctuations of the H−K distances of the three 4-ns MD simulations for the three P4-related systems. Obviously, the entrances of the ATP

(57) Humphrey, W.; Dalke, A.; Schulten, K. *J. Mol. Graphics* **1996**, *14*, 33−38.
(58) Hirschman, A.; Boukhvalova, M.; VanBruggen, R.; Wolfe, A. J.; Stewart, R. C. *Biochemistry* **2001**, *40*, 13876−13887.
(59) Marina, A.; Mott, C.; Auyzenberg, A. *J. Biol. Chem.* **2001**, *276* (44), 41182−41190.

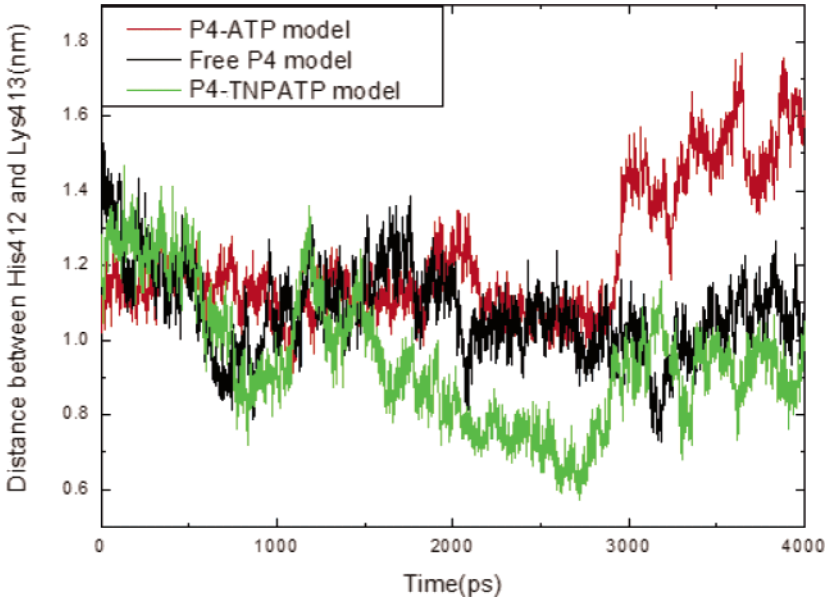

Figure 6. Time dependence of the minimal van der Waal distances between His413 and Lys494, which reflect the width of the binding pocket entrances for the three MD simulations.

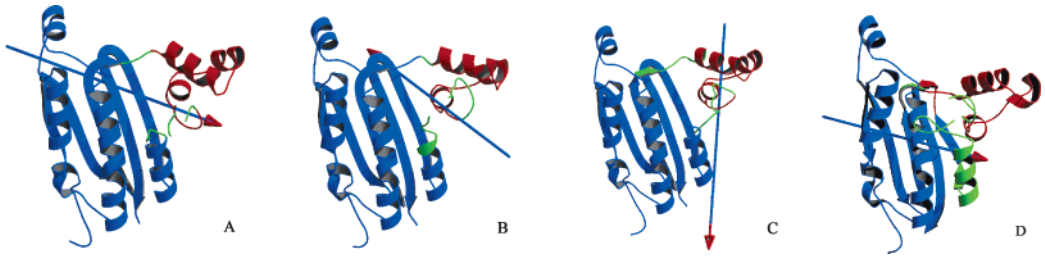

Figure 7. Principle-component mode of motion. (A−C) The first, second, and third motion modes of P4 in P−ATP complex. (D) The first motion mode of free P4. The colors of the arrows denote the particular moving domain (right-hand rule). The fixed domains (the large domains colored in blue) contain more than 130 residues including the residues from N terminal to the G1 box and those from the G2 box to C terminal, while the moving domains (the small domains colored in red) are composed of the residues after the G1 box to the middle of the F box, including less than 40 residues.

binding pockets of free P4 and P4−TNPATP did not open, for their H−K distances generally tends to decrease during the MD simulations. Differently, the H−K distance of P4−ATP complex fluctuates slightly around 11 Å from 0 to 3.0 ns; at ∼3.0 ns, the H−K distance suddenly increases up to ∼16 Å (Figure 6), and the ATP binding pocket holds to an open state till the end of the simulation. Similar to the X-ray crystal structure of the P4−TNPATP complex,[10,11] our MD simulation on the P4−ATP system shows that both His413 and Lys494 form hydrogen bonds with the ATP β-phosphate before 3.0 ns (Figure S4 in the Supporting Information). However, after 3.0 ns, His413 still forms a H bond with ATP; but the H bonds between Lys494 and ATP are broken, and Lys494 moves away from His413, opening the entrance of the ATP binding pocket (Figure S5 in the Supporting Information). It is interesting that the time when the entrance of binding pocket open aligns well with that of the conformational change of ATP (Figure 3A), indicating that the conformational switch of ATP correlates with closed-to-open change of the ATP lid: after ∼1.6 ns equilibrium, ATP converts to extended conformations from folded conformations, during this period HAA forms a hydrogen bond to O1B, and ATP acts like an elongated spring; at ∼3.0 ns, ATP gets back to folded conformations and the HAA···O1B H bond forms again, the "elastic force" of the elongated spring retraction ruptures the H bond between ATP and Lys494, leading Lys494 to move away and thus the ATP lid is opened. In contrast, TNPATP cannot change its conformation inside the binding pocket of P4−TNPATP complex due to lack of intramolecular H-bond breaking and making and there is no substrate stimulation in the free P4, ATP lids of these two systems do not open during the MD simulations. This verifies again the correlation between the ATP conformational change and the closed-to-open change of the ATP lid.

Correlation between ATP Conformational Change and the Motions of P4 Motifs. As the ATP binding pocket of P4 consists of several conserved motifs (Figure 1), the ATP conformational switch probably induces the movements of these motifs. To reveal the correlation between the ATP conformational switch and the motions of P4 motifs, PCA were performed based on the MD simulation results for both the P4−ATP complex and free P4, and corresponding motion modes were identified using the program DYNDOM.[55,60] The results are shown in Figures 7 and 8.

The first three largest eigenvalues for P4 in the P4−ATP complex account for ∼47% of total motions. Projections of the trajectory of P4 on the these three eigenvectors vs simulation time were calculated, as shown in Figure 8, indicating that the

(60) Hayward, S.; Lee, R. A. *J. Mol. Graph Model* **2002**, *21*, 181−183.

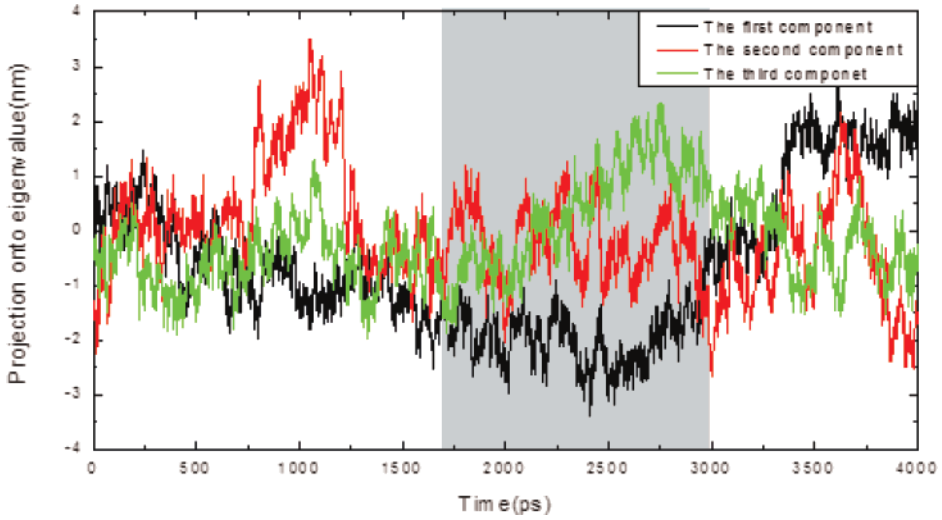

Figure 8. Projection of the main-chain atom trajectory onto the first three eigenvectors as a function of time.

first and third motion modes for P4 in P4−ATP complex are likely related to the ATP conformational switch, because the fluctuations of the eigenvalues corresponding to these two components are in good accordance with the conformational change profile of ATP (Figure 3A). However, comparison with the PCA result of free P4 reveals that the first component in P4−ATP is highly similar to that of free P4 (Figures 7A and 7D), suggesting that it is a fundamental motion of P4. Thus, we can conclude that the third component may truly correlate with the conformational dynamics of ATP in the binding site of P4. The effective hinge axis of the third component is almost parallel to the N box and perpendicular to the F box (Figure 7C). The displacement ratio of interdomain to intradomain of the third component is ∼1.88; the angle of rotation is ∼21.5°, which describes a clockwise pivoting motion of the F box toward the opposite side of the N box. This motion fitly leads the ATP lid to open up, widening the entrance of the ATP binding pocket. As will be discussed later, the P1 domain of CheA only binds to the ATP lid open conformation of P4, putting in practice autophosphorylation.

DYNDOM analysis discovered two key residues related to the motion of the third principle component, viz., Glu106 and Phe491. Glu106 acts as a mechanical hinge, whose C^{α} is 5.3 Å away from the axis and Phe491, a highly conserved residue in the F box, is a dominant contributor among the residues involved in the interdomain rotation and bending. The Φ and Ψ dihedral angles of Phe491 change by 25 and 52°, respectively. Therefore, it is expected that mutations on these two residues might affect the motion mode of the third component, leading to an inadequacy or disruption of CheA autophosphorylation function. Indeed, experimental data demonstrated that when the conserved Phe491 in *E. coli* was mutated to tyrosine, the rate of binding ATP only slightly decreased, by ∼1.67 times, but the rate of autophosphorylation was severely reduced to ∼2% of wild-type CheA.[58]

PCA was also performed on the MD trajectory of P4−TNP−ATP complex. The result is shown in Figure S6 in the Supporting Information, which indicates that the motion modes of P4 in P4−TNPATP complex are similar to that of free P4, implying that TNPATP cannot open the lid of pocket of P4 domain (see discussion below).

Correlation between Autophosphorylation and P1−P4 Binding. As mentioned above, autophosphorylation of CheA occurs between the P1 and P4 domains.[33] Therefore, investigation of the P1−P4 interaction is of significance for understanding the CheA autophosphorylation mechanism. Because the X-ray crystal structures P1 and P1−P4 complex of *S. typhimurium* are not available, we constructed a 3D model for P1 domain using the homology modeling method based on the X-ray crystal structure of the P1 domain of *S. typhimurium* and then generated a 3D structural model for the P1−P4 complex by using the protein−protein docking method 3D-DOCK.[36−38] The sequence alignment and structural superposition of the CheA P1 to the *S. typhimurium* P1 are shown in Figure S7 in the Supporting Information. The 3D model of P1 has a cylinder-like geometry with a diameter of ∼18 Å (Figure S7C in the Supporting Information), which is very close to the width of the binding site entrance of P4 in its open state. This suggests that the open state of P4 may be a good starting conformation of P4 for P1 docking. Two snapshots (2900 and 3045 ps, Figure S5 in the Supporting Information), respectively, representing closed and open states of P4 domain were extracted from the MD trajectory of P4−ATP complex. Possible 3D models of a P1−P4−ATP complex were constructed by docking P1 directly to the open and closed states of the P4−ATP complex using 3D-DOCK.[36−38] It was found that the top five candidates of the constructed models for proper P1−P4−ATP complexes were formed only by the open state of P4. From the five candidate models, the one with the lowest optimized energy was selected as an initial structure for further study. The optimized structure of P1−P4−ATP is shown in Figure 9 (left). The 3D model of the P1−P4−ATP complex indicates that His45 of P1 is near the terminal phosphate of ATP in the binding site of P4, posing a proper geometry for subsequent autophosphorylation (Figure 9 (right)).

To study the dynamics of the P1−P4 interaction, a 2-ns MD simulation was conducted on the 3D model of P1−P4-ATP complex. The RMSD of all C^{α} atoms of P1−P4−ATP complex converges to ∼2.5 Å after ∼0.5 ns of equilibrium (Figure S8 in the Supporting Information), suggesting that the structure of P1−P4−ATP complex is stable after 0.5 ns simulation. According to the structural model of the P1−P4−ATP complex

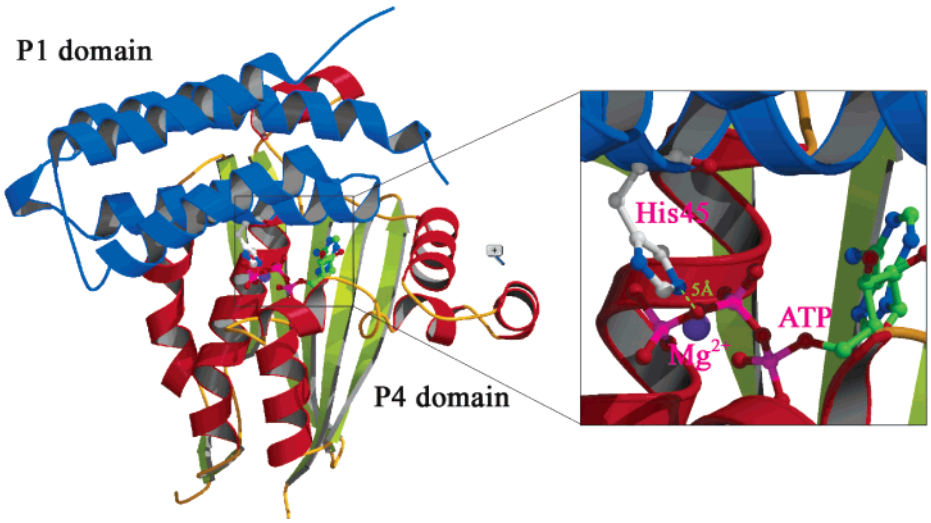

Figure 9. The 3D model of P1−P4 complex with ATP in the binding site of P4. Left picture is the ribbon representation of the whole structure of P1−P4 complex and right one is the enlargement for the structure of autophosphorylation site. ATP and His45 of P1 are displayed in ball and sticks. P1 and P4 are colored in blue and red, respectively. The green dash line stands for the distance between His45 and ATP.

(Figure 9) and experimental data,[61] the nitrogen atom at the imidazole ring of His45 of P1 and the oxygen atom O2C of ATP (Figure 3) are the reaction sites for the autophosphorylation. Accordingly, the profile of the distance between these two atoms (N−O distance) vs simulation time was monitored during the 2-ns MD simulation. The result is shown in Figure S9 in the Supporting Information. The N−O distance slightly fluctuates around 5 Å. This distance is favorable for ATP to transfer its terminal phosphoryl group to His45 of P1. It has been proposed based on the result of the kinetics analysis of CheA[24] that the P1−P4 complex has two forms: an inactive conformation with a weak binding between P1 and P4, and an activated conformation with a strong interaction and favorable geometry for phosphate transfer. Our MD simulation indicates that we have obtained the 3D model of an active form of P1−P4 complex.

TNPATP Inhibits P1−P4 Binding. MD simulation revealed that His413 always H bonds to Lys494 in the P4−TNP−ATP complex during the simulation time (Figure S10 in the Supporting Information), indicating that the ATP lid of P4−TNPATP complex cannot open. The reason is that the conformation of TNPATP is not capable of shrinking (parts A and C of Figure 3). Because the ATP binding pocket of P4−TNPATP complex is always at the closed state, P1 cannot bind tightly with P4. In addition, the phosphate tail of TNP−ATP cannot stretches into the G2 box (Figure S10 in the Supporting Information), where it is presumed to be the place for autophosphorylation.[20] Therefore, the phosphoryl group of TNPATP cannot access His45. This may be the reason that TNPATP is not an agent but an inhibitor for phosphorylation.[21]

Discussion

As mentioned above, CheA is a core protein in the signaling pathway of class II TCSs.[12] In general, CheA consists of five domains (P1−P5), and autophosphorylation occurs between P1 and P4 domains. In this study, we have obtained the dynamics process of P4 induced by the conformational switch of ATP, the closed-to-open change of the ATP lid in particular, and the P1−P4 binding model with molecular modeling and dynamics simulations, and thus we can gain some insights into the autophosphorylation mechanism at the atomic level.

Because of the intrinsic nature in comparison with P4 inhibitor such TNPATP, ATP may adopt two kinds of conformations inside the binding pocket of P4 by intramolecular H-bond breaking and making between HAA and O1B (Figures 3 and 4). Thus ATP switches between extended and folded conformations. Quantum chemical calculation indicated that the folded conformations of ATP is ∼6.40 kcal/mol more stable than the extended conformations (Figure S3 in the Supporting Information), thereby ATP poses as a folded conformation in the X-ray crystal structure of the P4−ATP complex. However, MD simulation addressed that a water molecule (Wm) gradually inserts between HAA and O1B and forms a H-bond bridge with these two atoms; thus ATP is spread into extended conformations for a while (Figure 5). The energy increase of ATP from folded conformations to extended conformations is compensated by the H-bond bridge. In addition, the water insertion decreased the activation energy ∼4.33 kcal/mol for the ATP conformational change (Figure S3 in the Supporting Information). On the reverse process, ATP shrinks back to folded conformations by the drive of energy difference. The conformational change of ATP matches well with the conformational fluctuation of P4 (Figure 3B), indicating that the conformational change of P4 may be driven by the ATP conformational switch. Indeed, ATP shrinking at ∼3 ns ruptures the H bond between ATP and Lys494, leading Lys494 to move away, and thus the ATP lid is opened out (Figure 6). The importance of Lys494 of the conserved motif to the activity of histidine kinase autophosphorylation has been demonstrated by mutagenesis study.[59] Interestingly, MD simulations indicated that the ATP lids of both free P4 and P4−TNPATP are always kept as closed states, suggesting that stimulating conformational change of P4 is a special functionality of ATP. In addition, PCA results illustrated that only the MD trajectory of the P4−ATP complex rather than the MD trajectories of free P4 and P4−TNPATP complex included the movement (the third component) corre-

(61) Hongjun, Z.; W. F. *Biochemistry* **1997**, *36*, 699−710.

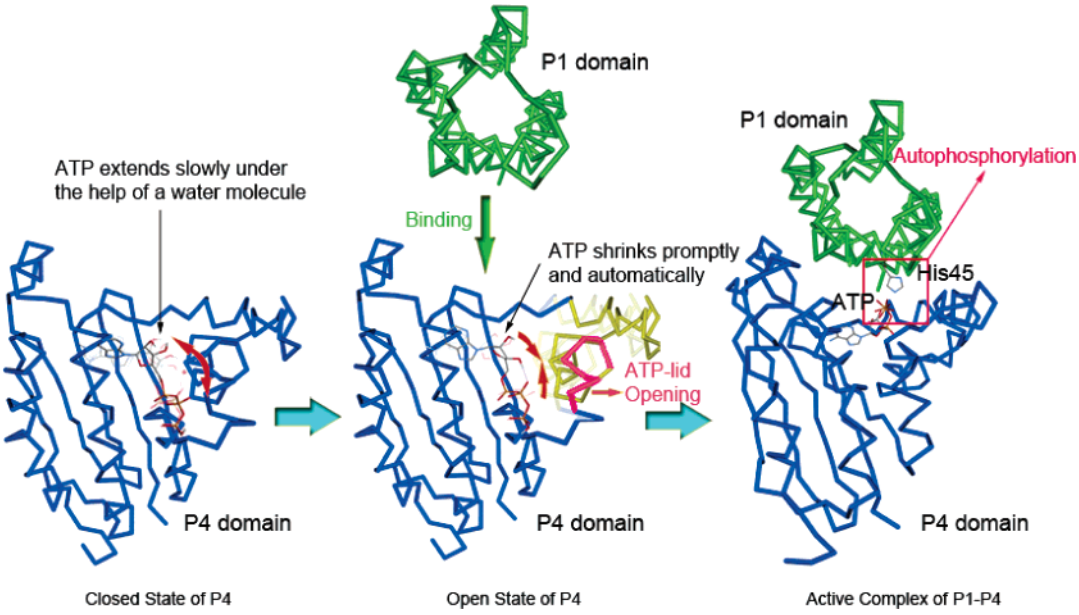

Figure 10. A postulated mechanism for the autophosphorylation of CheA histidine kinases.

sponding to the opening of the ATP lid (Figures 7 and S10 in the Supporting Information), implying again the specificity of ATP.

Protein−protein docking simulations indicated that P1 fitted well with the open state of P4 (Figure 9 (left)). Nevertheless, P1 could not match complementarily with the closed state of P4. This result is in agreement with the kinetic and thermodynamic determination for P1−P4 binding.[24] The P1−P4 complex indicated that His45 of P1 situated a favorable position for phosphorylation by ATP bound in P4, the distance between the nitrogen atom at the imidazole ring of His45 of P1 and the oxygen atom O2C of ATP (N−O distance) is ∼5.0 Å (Figure 9 (right)). MD simulation on the P1−P4−ATP complex demonstrated that the N−O distance is very stable (Figure S9 in the Supporting Information). This indicates that the conformational switch of ATP is directly correlative to P1−P4 binding and thereby the CheA autophosphorylation, i.e., ATP is not only a phosphoryl group donor but also an activator for CheA phosphorylation.

On the basis of our modeling and simulation results and analyses, we may propose an atomic mechanism for the CheA autophosphorylation as indicated in Figure 10. (1) By binding to the ATP pocket of P4 with a folded conformation, ATP may stretch into extended conformations under the help of a water molecule by forming a H-bond bridge to HAA and O1B (Figure 3), which lowers the activation energy by ∼4.33 kcal/mol for the ATP conformational change; at the same time, ATP forms two H bonds with His413 and Lys494 all the while. (2) Because of the stability of the folded conformations, ATP tends to shrink back to folded conformations by recovering its intramolecular H bond. (3) The "elastic force" for ATP shrinking suddenly ruptures the H bond between ATP and Lys494; thus Lys494 is allowed to move away from the ATP binding pocket entrance, and the ATP lid opens up. (4) Finally P1 binds tightly with the open state of P4, and thus His45 of P1 could be phosphorylated by ATP.

Conclusions

The present molecular modeling and MD simulations have provided a new insight into the autophosphorylation mechanism of CheA at the atomic level (Figure 10). The MD simulations clearly addressed the dynamic behavior of the CheA P4 domain induced by ATP conformational switch inside the binding pocket, which is totally different from those of both free and inhibitor bound P4 domains. Distinct difference existing in dynamics of free, ATP-bound, and TNPATP (inhibitor)-bound P4 domains is that ATP is able to switch between folded and extended conformations, pushing the ATP lid to open up. Another notable finding from the MD simulations is that P1 may only bind tightly to the open state of P4 (Figure 9), implying that only the P4−ATP complex is capable of binding P1. This demonstrates the experimental fact that TNPATP is an inhibitor of CheA autophosphorylation although it is an analogy of ATP. Conformational switch of ATP is the root for all the distinguishing characters of the P4−ATP complex. One water molecule (Wm) plays an important role in the conformational changes of ATP inside the binding pocket of P4 (Figures 5 and S3). Finally, an autophosphorylation mechanism of CheA is postulated whereby the ATP conformational switch stimulates the opening of the ATP lid, which is beneficial to P1 binding, and thus autophosphorylation occurs between P1 and P4. Accordingly, we can conclude that ATP is not only a phosphoryl group donor but also an activator for CheA phosphorylation.

Acknowledgment. This work was supported by grants from the State Key Program of Basic Research of China (2002CB-512802, 2004CB518901) and Shanghai Science and Technology Commission (03DZ19228). We thank Shanghai Supercomputer Center for its support.

Supporting Information Available: Computational procedure is available in Figure S1. Binding modes of ATP and ADP−CP to P4 are available in Figure S2. Reaction pathway of the ATP conformational change for a folded conformation to an

extended conformation is available in Figure S3. Number of H bonds between doorkeepers and ATP is available in Figure S4. Process of opening the ATP lid of binding site is available in Figure S5. The first motion mode of P4 in P4−TNPATP complex is available in Figure S6. Alignment sequence between CheA P1 domain of *T. maritime* and CheA P1 domain of *Salmonella typhimurium* for homology modeling is available in Figure S7. C^{α} RMSD of the combined structure of P1 and P4 relative to the initial structure conformation of simulation is shown in Figure S8. Distance between reaction points for phosphorylation in P1−P4 complex is shown in Figure S9. Directly interaction between His413 and Lys494 in the P4−TNPATP model is shown in Figure S10. This material is available free of charge via the Internet at http://pubs.acs.org.

JA051199O